Multiparameter Remote Contact Force Sensor With Embedded Bend Sensing for Tendon-Driven Hand Robots

Sang-Hun Kim, Useok Jeong, and Kyu-Jin Cho, *Member, IEEE*

***Abstract*—Integrating multiple sensors without increasing the structural complexity and their original form factor is a major concern in robotic applications, particularly in tendon-driven systems. This study proposes a multiparameter contact force sensor with bend sensing by utilizing an improved Bowden cable design. The proposed sensor consists of an end tip with an elastomer membrane, a Bowden cable consisting of a sheath and dual inner wires, and a remotely separated sensing component. The electrical wirings are decoupled from the mechanical Bowden cable system. The displacement difference between the force-sensing and bend-sensing wires is transmitted through the sheath, indicating the contact force on the end tip. The modeling and experiments verify that the contact force applied on the end tip is linearly related to the sensor output signal and is reliable after repeated measurements. The proposed sensor, utilizing the flexible Bowden cable as its sensing modality, can be integrated into a diverse range of tendon-driven robotic applications. These applications include a robotic hand with tactile and angle sensing capabilities, as well as a soft wearable robot for the hand (Exo-glove Poly II). The compact form factor of the proposed sensor enables geometric sensing without increasing structural complexity for multiparameter sensing in robotic applications.**

***Index Terms*—Bowden cable, contact force sensor, flexible sensor, soft wearable robot, tendon-driven robot.**

Manuscript received 17 December 2022; revised 14 March 2023; accepted 10 May 2023. Recommended by Technical Editor Giuseppe Carbone and Senior Editor Qingze Zou. This work was supported in part by the National Research Foundation of Korea funded by the Korean Government (MSIT) under Grant RS-2023-00208052, and in part by the Korea Institute of Industrial Technology "Development of Soft Robotics Technology for Human-Robot Coexistence Care Robots" under Grant KITECH EH230015. *(Corresponding author: Kyu-Jin Cho.)*

Sang-Hun Kim and Kyu-Jin Cho are with the Biorobotics Lab, Soft Robotics Research Center, SNU-IAMD, Department of Mechanical Engineering, Institute of Engineering, Seoul National University, Gwanak-gu 08826, South Korea (e-mail: pine6710@snu.ac.kr; kjcho@snu.ac.kr).

Useok Jeong is with the Robotics R&D Group, Korea Institute of Industrial Technology, Cheonan-si 31056, South Korea (e-mail: usjeong@kitech.re.kr).

This article has supplementary material provided by the authors and color versions of one or more figures available at https://doi.org/10.1109/TMECH.2023.3281062.

Digital Object Identifier 10.1109/TMECH.2023.3281062

I. Introduction

VARIOUS types of sensors have been applied in robots to facilitate position perception and safe interaction with the surroundings [1], [2], [3]. Extensive efforts have been made to develop multiparameter sensors that incorporate different sensing mechanisms or use the same sensing element. A heterogeneous sensing structure that employs an optical sensing mechanism and gold nanowire strain gauges to distinguish bending from compression was proposed in a previous study [4]. Compact form factor sensors have been developed by combining optoelectronics, microfluidics, and piezoresistivity with artificial neural networks to classify and decouple multimode deformations [5]. Bending and compression force-sensing structures with a conductive elastomer [6] or multiple fluidic channels [7] were designed to geometrically decouple the sensing elements.

Incorporating multiparameter sensors into robots requires high-level integration as it involves the installation of multiple sensing devices with signal and power cables that must be distributed through the complicated mechanical structure of the robot. Hence, previous studies have suggested sophisticated mechanical designs that targeted specific sensor form factors to facilitate integration and enhance the robust interconnection of the system. A sensor-integrated soft prosthetic hand was demonstrated by implanting pressure and strain sensors between the soft layers of the fingers and covering them with the outer skin [8]. Scalable artificial fingers were presented using a parametrized model with a modular multimodal sensor system [9].

Tendon-driven robots used compact, soft, and lightweight applications, such as robotic hands, wearable robots, and surgical robots, are limited by sensor integration issues [10], [11], [12], [13], [14]. Tawk et al. [15] proposed a tendon-driven 3-D printed soft monolithic robotic finger integrated with pneumatic sensing chambers and electric components of pressure sensors for sensing bending position and touch. Placing sensors on the end-effector or inside the tendon-driven robot structure increases the size of the robot; thus, losing the advantage of the tendon-driven mechanism. It also severely damages the electric components of the sensors due to physical contact or contact with water. To address these challenges, some studies suggest the extension of the mechanical stimuli to the remotely separated electrical sensing part, with the goal of increasing compactness and avoiding interconnection issues at the end-effector.

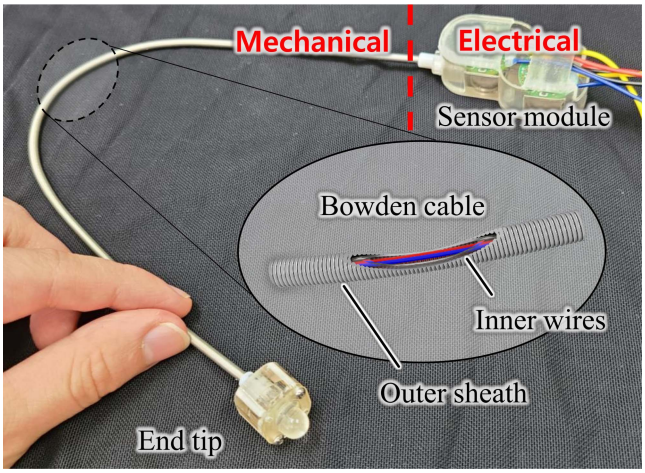

Fig. 1. Prototype of a remote contact force sensor with bend sensing (BoAF sensor: Bowden cable Angle and Force sensor). The sensor is divided into a mechanical sensing part and an electrical sensing part.

A magnetoresistive sensor with a remote touch tip for tactile sensing was proposed to isolate the sensor electronics from the end-effector [16]. However, an optimized joint design and tightly sealed touch tip structures are required to prevent air leakage when integrating the sensor into the tendon-driven gripper [17].

Integrating optical fiber sensors that measure changes in light intensity, phase, or wavelength is another approach that can be used. Optical fiber sensors possess the advantages of a small size that makes integration with a compact form factor and soft and lightweight applications feasible [18]. Previous studies on catheters with optical fiber sensors show high resolution and accuracy in measuring catheter tip force under silicone or biofluid-filled environments [19], [20]. Kesner et al. [21], [22] designed a cardiac catheter that consists of a sheath, a guidewire for the tendon drive system, and an end-effector to compensate for the heart motion and regulate the forces applied to the tissue. However, for integrating optical fiber sensors into the end-effector, two additional independent optical fibers are required to emit and receive light signals; moreover, digital acquisition with a high-cost digital fiber amplifier is needed to interpret the signals from the fiber optic sensor.

In a previous study, we demonstrated a low-cost, large curvature bend sensor based on a Bowden cable [23], [24]. The proposed sensor utilized a Bowden cable as its sensor modality. Bowden cables are widely used tendon-driven mechanisms and consist of an inner wire and an outer sheath that transmits force through the inner wires. The flexibility of the Bowden cable is suitable for various robotic applications that require transmission paths with complex and varying shapes. This enables actuators to be placed away from the end-effector, reducing the robot's weight, size, and complexity.

In this study, we propose a multiparameter remote sensor that detects the contact force depending on the bending angles in a compact form factor by adopting the mechanical characteristics of a Bowden cable for integration into tendon-driven robots, as shown in Fig. 1. The sensor adopts the form factor of a spring sheath, enabling it to integrate with additional sensing wires along the existing tendon path, thus embedding itself in a tendon-driven robot, as illustrated in Fig. 2. The proposed sensor measures the geometric change in the relative displacement and translates it into the contact force depending on the bending angle to separate the sensor electronics from the robot structure. The electronics are decoupled from the mechanical Bowden cable system [23], [25]. The principle of the proposed sensor is to mechanically convert the contact into the displacement of the sensing wire. The contact force is calculated by compensating for the sensor's measured bending angle. As there are various options for displacement transducers, users can choose one based on their preference, without complex signal processing. The sensors are implemented as tactile and proprioceptive sensors in tendon-driven mechanisms used in robotic hands and soft wearable robots.

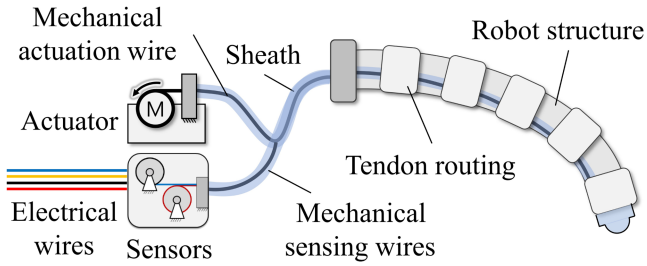

Fig. 2. Overall structure of tendon-driven system integrated with the proposed sensor.

The rest of this article is organized as follows. The concept and basic design of the proposed sensor are described in Section II. In Section III, the force characteristic modeling of the sensor to estimate the sensor characteristics is introduced. The characterization of the proposed sensor based on experimental results is discussed in Section IV. Finally, Section V describes the prototype development for robotic applications. Finally, Section VII concludes this article.

II. Concept and Design

A. Sensing Principle

The geometric sensing principle of the proposed sensor is based on the mechanical transmission of the displacement difference of the contact point by the wires and the remote sensor. Previous studies have proved a linear relationship between the bending angle and sensor output of the helical coil sheath within the allowable range of curvature, as shown in (1)–(3) [23]. Each helical coil maintains contact inside the curvature, and the gap outside the curvature increases as shown in Fig. 3

$$\Delta l = \frac{aL}{b}\sqrt{2\left(1-\cos\left(\frac{b}{L}\theta\right)\right)} \tag{1}$$

$$\kappa = \theta/L \tag{2}$$

$$\Delta l = \frac{a\sqrt{2(1-\cos(b\kappa))}}{b\kappa}\theta \approx a\theta. \tag{3}$$

In the equations, κ is the bend curvature of the helical coil sheath, θ is the total bending angle, l is the length of the inner wire, L is the total length of the sheath, a is the helical

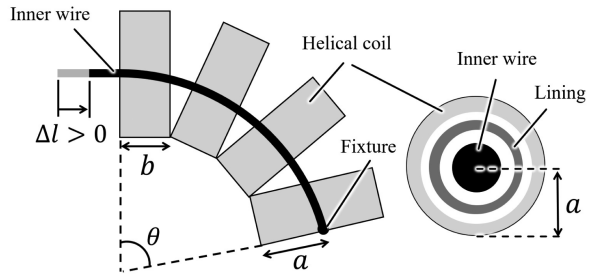

Fig. 3. Basic principle of the proposed sensor using a Bowden cable.

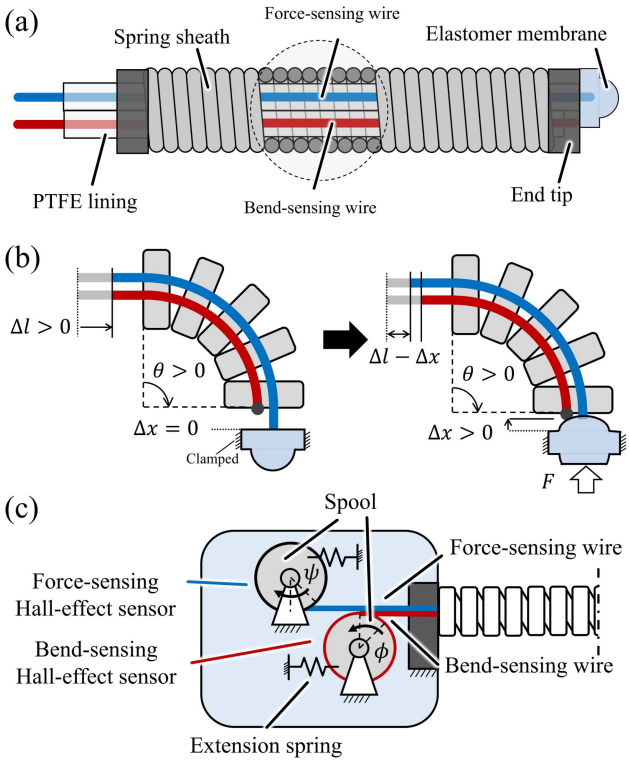

Fig. 4. Schematic of the proposed sensor sheath and end tip: (a) a cross-sectional view of the sheath comprising a helical coil, two mechanical sensing inner wires, and PTFE lining, (b) displacement difference between mechanical sensing inner wires due to contact force on the end tip with bending angle θ, and (c) top view of the sensor module comprising spools extension springs and Hall-effect sensors with measured angles of ψ and ϕ for force-sensing and bend-sensing, respectively.

coil radius, and b is the coil wire diameter of the sheath. The nonlinear term in (32) is approximated as a linearization term, representing the linear relationship between the bending angle and the displacement difference of the inner wire since b is smaller than L.

B. Mechanical Design of the Sensor

The proposed sensor comprises three parts: a sheath to transmit the displacement difference, an end tip for the contact, and a sensor module with dual Hall-effect sensors. The sheath contains two sets of inner wires and linings for the displacement difference, as shown in Fig. 4(a). The bend-sensing inner wire (colored in red in Fig. 4) is pulled when the sheath is bent, which can be used to detect the bending of the sheath. The force-sensing

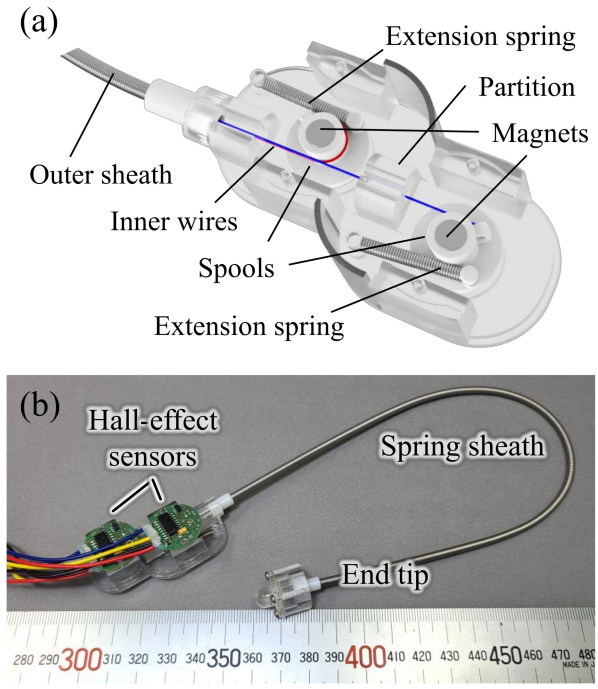

Fig. 5. Prototype of the proposed sensor: (a) computer-assisted design of the sensor module, and (b) overall view of the sensor comprising a sensor module with two Hall-effect sensors, spring sheath, and an end tip.

inner wire (colored in blue in Fig. 4) is pushed by the end tip and transmits the displacement difference to the sensor. The end tip contains an elastomer membrane that deforms with contact and is connected to the force-sensing wire. The sensor module contains two Hall-effect sensors, each with a spool connected to bend-sensing and force-sensing wires, as shown in Fig. 5. The bend-sensing wire wraps around the spool and rotates it counterclockwise when the sheath bends. The force-sensing wire is connected to the spool, causing it to rotate clockwise when the end tip is pressed. The sensor module also has extension springs that generate the passive torque of the spool and tension to the sensing wires. The extension springs provide initial tension for the inner sensing wires, preventing slack inside the sheath and enabling accurate measurement of the displacement difference of the end tip. The absence of initial tension would hinder the transmission of displacement difference while the lack of kinking resistance of the wire could cause loose sensing wires.

C. Sensor Prototype

The overall structure of the proposed contact force sensor with an embedded bend sensing prototype has the form factor of a Bowden cable with an outer diameter (a) of 3 mm, an inner diameter (L) of 2.4 mm, and a length of 300 mm. Therefore, the spring sheath can be cut into the desired length of the sensor and is made of stainless steel to ensure good robustness under different environmental conditions. Two polytetrafluoroethylene (PTFE) linings of diameter ϕ0.6 mm were embedded inside the spring sheath to reduce friction along the inner wires. These PTFE linings were twisted inside the sheath, and the polymer

inner wires (Dyneema) passed through the linings. A polymer wire (ϕ0.24 mm) with a high modulus (tensile modulus of 109–132 GPa) was used for bend sensing to prevent elongation of the wire. Additionally, it can be easily wound on a spool, and the wire tightly fits the end tip for secure positioning. A NiTi superelastic wire (ϕ0.35 mm) was embedded in a spring sheath with kink resistance and low friction between the inner linings.

The end tip of the sensor contains a polydimethylsiloxane (PDMS) (Dow Corning Corp., Sylgard 184) membrane with a hemispherical shape. The PDMS base and cross-linker were mixed in a ratio of 10:1 and cast using a concave hemispherical mold. The bottom of the elastomer membrane was connected with the force-sensing wire that passes through a spring sheath. The membrane was clamped as the cover was assembled to the end tip.

The sensor module utilizes Hall-effect angle sensors and magnets to measure the rotation angle of the spool with a radius of 3 mm. Extension springs with an outer diameter of ϕ2.3 mm were attached between the spools and the frame to provide passive torque to the spools and tension to the sensing wires. Bearings were assembled with the spools to reduce friction on the shaft. The Hall-effect sensor (RMB20IC12BC10, RLS) has a resolution of 4096 counts per turn (0.088° per count), an accuracy of $\pm$0.5°, and a hysteresis of 0.18°.

III. Modeling for Contact Force Sensing

This section describes the model for the force characteristics of the proposed sensor, which is derived from the displacement of the inner wires. The resultant model estimates the force sensing resolution for a bending angle of the sensor and shows that the contact force and sensor output are linearly related.

A. Displacement Difference Relationship of Inner Wires

The relationship between the displacement difference of the bend-sensing and force-sensing wires is shown in the following:

$$r\Delta\phi = \Delta l_{\text{bend}} = a\theta \tag{4}$$

$$r\Delta\psi = \Delta l_{\text{force}} = \Delta x + a\theta \tag{5}$$

$$\Delta x = \Delta l_{\text{force}} - \Delta l_{\text{bend}} \tag{6}$$

where l_{bend} is the length of the bend-sensing wire, l_{force} is the length of the force-sensing wire, k_{tip} is the stiffness in the normal direction of the membrane, r is the radius of the spool, x is the displacement of the membrane, ψ is the rotation angle of the spool connected to the force-sensing wire, and ϕ is the rotation angle of the spool that winds around the bend-sensing wire.

B. Friction Model Along the Sheath

The proposed sensor comprises an inner wire that transmits the force and a sheath that supports the tension of the inner wire and guides its base according to the principle of the Bowden cable, resulting in friction between the inner wire and the sheath. The force distribution of the inner wire along the sheath is derived below using the Capstan equation [26]

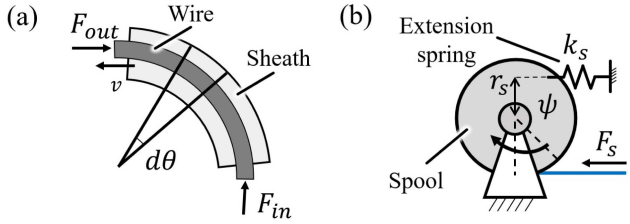

Fig. 6. Description of the modeling parameters: (a) friction model along the Bowden cable, and (b) spool connected by the force-sensing wire and extension spring in the sensor module.

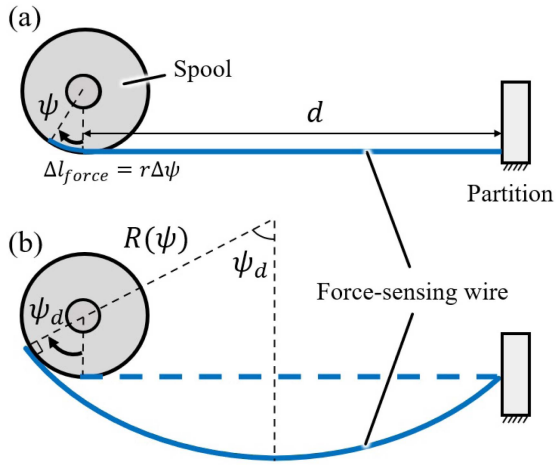

Fig. 7. Schematic diagram of the spool and force-sensing wire of the sensor module, (a) linear region before the detachment angle, (b) nonlinear region after the detachment angle; the blue solid line represents a curved force-sensing wire, which results in the nonlinear region. Schematic diagram of the spool and force-sensing wire in the sensor module: (a) linear region before the detachment angle, and (b) nonlinear region after the detachment angle. The blue solid line represents a curved force-sensing wire, which results in the nonlinear region.

$$\frac{F_{\text{out}}}{F_{\text{in}}} = e^{-\mu\theta\cdot\text{sgn}(v)} \tag{7}$$

where F_{in} is the input force applied on the end tip, F_{out} is the output force applied to the sensor module, μ is the coefficient of kinetic friction between the sheath and the wire, θ is the total bending angle of the sheath, and v is the velocity of the wire relative to the sheath. $\text{sgn}(v)$ is 1 and -1 under the loading and unloading conditions, respectively, as shown in Fig. 6(a).

C. Advanced Model Considering Friction Hysteresis

Based on the relationship between the displacement difference of the inner wires and that of the friction model obtained by the Capstan equation, the force equilibrium of the end tip is derived as

$$F = k_{\text{tip}}\Delta x + F_{\text{in}} = k_{\text{tip}} r\Delta(\psi - \phi) + F_{\text{in}} \tag{8}$$

where F is the contact force applied on the end tip.

In the sensor module, the extension spring applies tension to the force-sensing wire. The tension on the force-sensing wire is

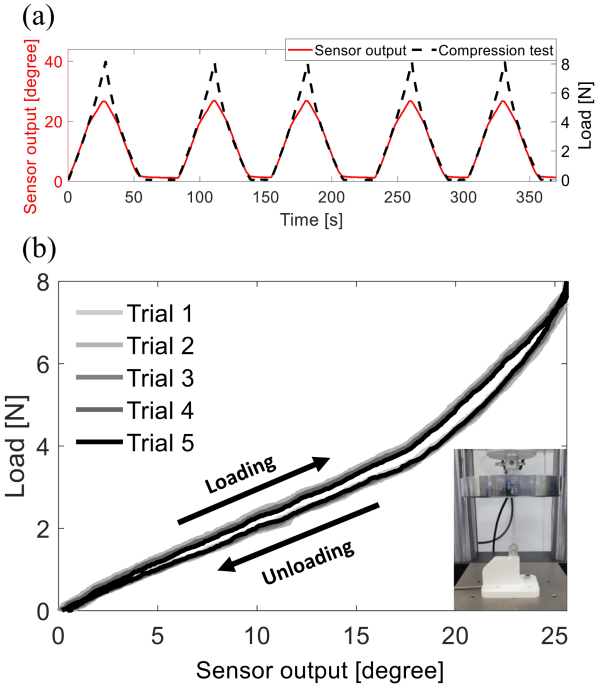

Fig. 8. Experimental results for the compression test: (a) time-domain results, and (b) repeated measurements in the sensor output domain.

expressed as

$$F_s = \frac{\tau_s}{r} = k_s \frac{r_s^2}{r} \Delta(\psi_0 - \psi) \tag{9}$$

where F_s is the spring force applied to the inner wire, τ_s is the spool torque because of the extension spring, and k_s and r_s are the spring coefficient and distance from the center of the spool to extension spring, respectively, as shown in Fig. 6(b)

$$F_s + F_{\text{out}} = f_{\text{sensor}} \cdot \text{sgn}(v). \tag{10}$$

The force equilibrium of the sensor module is derived as (10), where f_{sensor} is the friction at the sensor module.

The relationship between the input and output forces through the Bowden cable is derived from the Capstan equation in (7). A hysteresis that causes the transient change of input force between $F_{\text{out}}e^{\mu\theta}$ and $F_{\text{out}}e^{-\mu\theta}$ exists due to the friction, depending on the moving direction of the wire

$$F_{\text{in}} = F_{\text{out}} e^{\mu\theta \cdot \text{sgn}(v)}. \tag{11}$$

The contact force at the end tip is derived using (8)–(11) as a function of ψ and ϕ

$$F = k_{\text{tip}} r \Delta(\psi - \phi) + (f_{\text{sensor}} \cdot \text{sgn}(v) - F_s) e^{\mu\theta \cdot \text{sgn}(v)}. \tag{12}$$

In the constant bending angle condition, (12) is converted to a linear equation of $\Delta\psi$, as shown in (13). Modeling under the quasi-static condition, in which the bending angle is constant or almost unchanged ($\Delta\phi$ becomes zero), indicates that the proposed sensor has linearity between the contact force and sensor output signal

$$F = \begin{cases} \left(k_{\text{tip}} r + k_s \frac{r_s^2}{r} e^{\mu\theta}\right) \Delta\psi + f_{\text{sensor}} e^{\mu\theta}, & \text{if } v > 0 \\ \left(k_{\text{tip}} r + k_s \frac{r_s^2}{r} e^{-\mu\theta}\right) \Delta\psi - f_{\text{sensor}} e^{-\mu\theta}, & \text{otherwise.} \end{cases} \tag{13}$$

D. Nonlinearity Calibration

The bend-sensing wire of the proposed sensor has low bending stiffness and is easily wound on a spool, ensuring linearity in its displacement variation. Conversely, the force-sensing wire is kink-free and can be detached from the spool when the rotation angle exceeds the detachment angle (ψ_d) of the spool, as shown in Fig. 7. Therefore, the nonlinearity in the sensor output is caused by converting the displacement variation of the force-sensing wire into the angle of rotation of the spool.

Experimental results showed that there are nonlinear characteristics between the load and sensor output beyond the detachment angle of the force-sensing wire, which depends on the bending stiffness of the wire material. To characterize the nonlinear region, Δl_{force} is calibrated in (5). Assuming that the curvature of the wire is circular, Δl_{force} is approximated using (14), where $R(\psi)$ is the hypothetical radius of the force-sensing wire, and d is the length between the spool and partition, which is 8 mm in the design of the sensor module

$$\Delta l_{\text{force}} \approx r\Delta\psi + 2\Delta(R(\psi)\psi) = r\Delta\psi + \Delta\left(\frac{d}{\sin\psi} \cdot \psi\right). \tag{14}$$

IV. Characterization of the Sensor

In this section, we present the force characteristics of the proposed sensor tested at a constant bending angle. This section focuses on the force characteristics of the sensor since the bending characteristics have been extensively studied in a previous work [23].

A. Force Characteristics of the Proposed Sensor

The sensor prototype was characterized by applying compression at a constant bending angle. The sensor end tip was assembled with a 0.8-mm-thick membrane, and the extension spring was assembled with a spool. The constant bending angle of the sensor was 90°. The results obtained using the sensor and tensile testing machine are shown in Fig. 8(a) in the time domain.

Fig. 8(b) shows the repeated measurements of the sensor output during a complete span cycle. The average nonrepeatability (i.e., the maximum difference in the output when the same force is repeatedly applied) of the compression load (applied five times) was 7.5×10^{-2}°, which was 0.59% that of the sensor output. The gradient of the average measured data was 0.211 $N/^\circ$ and 0.189 $N/^\circ$ under loading and unloading conditions, respectively, and the difference of 11.2% was because of hysteresis. The hysteresis (i.e., the maximum difference in the sensor output under the loading force when the force is increased and then decreased during a complete span cycle) was measured as 9.8% in the full scale. The average R-square value of the linear relationship between the loading force and sensor output was

TABLE I
SPECIFICATIONS OF THE PROPOSED SENSOR PROTOTYPE

Characteristic	Specification
Force-sensing range	$0-8\ N$
Force-sensing resolution	$0.016-0.02\ N$
Bend angle sensing range	$0-180°$
Bend angle sensing resolution	$0.6°$
Cost of the sensing structure	Low (Less than $10)

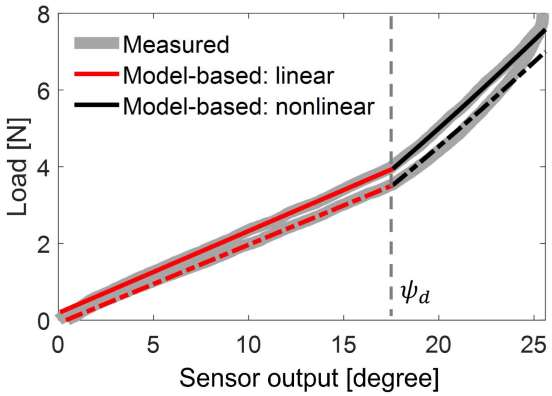

Fig. 9. Comparison of average measured experimental results (gray line), model-based prediction results in the linear region (red line), and in the nonlinear region (black line). The solid lines represent the results of force loading, and the dotted lines represent the results of unloading.

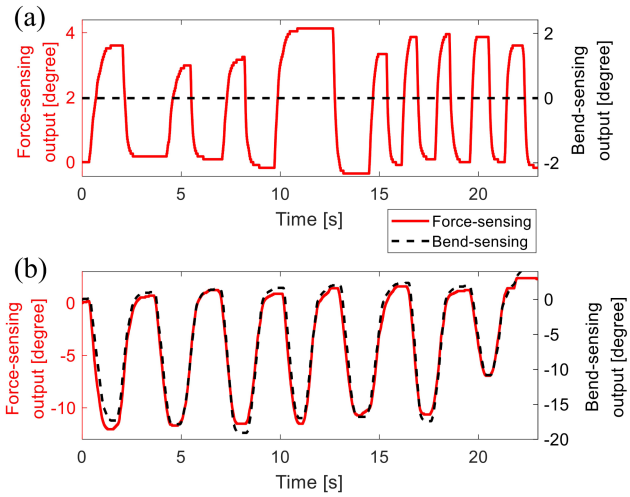

Fig. 10. Experimental results of crosstalk between force and bend sensing in the time domain. (a) Varying contact force with constant bending angle. (b) Varying bending angle with no contact force. The red solid lines represent the sensor output for force-sensing, and the black dotted lines represent the sensor output for bend-sensing.

0.9986, and that between the unloading force and sensor output was 0.9989 up to 17.8°. Table I lists the detailed specifications of the proposed sensor prototype.

B. Model-Based Prediction

A comparison of the experimental results and model-based prediction results obtained using (13) is summarized in Fig. 9. The average measured experimental result of Section IV-A is represented by the color gray. The model-based prediction result is divided into two regions: the linear region before the detachment angle (ψ_d) and the nonlinear region after the detachment angle. The solid and dotted lines denote the results for loading and unloading, respectively.

The parameters used for the model-based prediction are estimated as follows: the stiffness of the membrane (k_{tip}) is 3.78 $N/$mm, the stiffness of the extension spring (k_s) is 0.05 $N/$mm, the radius of the spool (r) is 3 mm, the distance to extension spring (r_s) is 6 mm, and the force-sensing wire detachment angle (ψ_d) is 17.8°. Moreover, friction estimation is necessary for the proposed sensor because the friction resulting from the bending angle of the sheath affects the force characteristics. The coefficient of friction (μ) between the force-sensing wire and the PTFE lining sheath was experimentally measured for different bending angles of the proposed sensor. For the friction estimation, additional compression tests were conducted. The extension spring of the spool was temporarily removed from the sensor module to focus on the friction effect of the Bowden cable and the sensor module. The coefficient of friction between the force-sensing wire and the PTFE lining (μ) was estimated as 0.264, which is the average value under the loading and unloading conditions, and the friction on the sensor module (f_{sensor}) was estimated as 1.19 N from the difference in the loading and unloading forces at a bending angle of 0.

Compared with the averaged experimental results, the model-based prediction results of the linear region indicate that the gradient of the model-based results was 0.215 $N/°$ and 0.204 $N/°$ under loading and unloading conditions, respectively, and the RMS errors were 0.050 N and 0.049 N, respectively. The model-based prediction results indicate that the extension spring in the sensing module reduces the hysteresis of the proposed sensor, where the hysteresis with the extension spring is estimated as 8.5%, and the hysteresis without the extension spring is estimated as 29.5%. In the nonlinear region, the gradient of the model-based results increases to 0.449 $N/°$ and 0.433 $N/°$ under loading and unloading conditions, respectively. The RMS errors between the experimental and model-based prediction results of the nonlinear region are 0.116 and 0.347 N under loading and unloading conditions, respectively. The results demonstrate the accuracy of the proposed model in predicting the behavior of the proposed sensor in both linear and nonlinear regions.

C. Crosstalk

The performance of multiparameter sensors is significantly affected by crosstalk between parameters. To assess the coupling between force and bend sensing, experiments were conducted under two conditions: varying contact force with a constant bending angle, and varying bending angle with no contact force. The results, as shown in Fig. 10(a), indicate that the bend-sensing wire has no effect even though the force-sensing wire travels through the Bowden cable when a contact force is applied.

Furthermore, a linear regression analysis of the experimental data in Fig. 10(b) shows that both the bend-sensing and force-sensing wires demonstrate a high degree of correlation, with a coefficient of determination $r^2 = 0.984$ when sensing wires travel through the Bowden cable during bending and

under varying bending angles with no contact force. The linear equation derived from the regression analysis is $\phi = 0.632\ \psi + 0.310$, recalling that ψ represents the force-sensing output and ϕ represents the bend-sensing output. This suggests that, despite the bending of the sensor, contact force can be accurately sensed by calibrating the linear relationship between the bend-sensing and force-sensing output. Overall, the results demonstrate that the proposed multiparameter sensor has minimal crosstalk between force and bend sensing, indicating that it can accurately measure both parameters simultaneously.

D. Reliability

The practical use of sensors requires the characterization of their reliability. Some studies on flexible sensors using liquid metal demonstrated reliable operation up to 10 000 cycle repetitions, but performance degradation was also noted [27], [28], [29]. Wire or tendon transmission suffers from reliability issues, particularly due to friction between the wire and sheath, causing significant fluctuation of the wire tension and accelerating the stress fatigue [30]. The reliability of wire transmission is determined by failures along the wire due to cyclic loading [31]. The life cycle of wire transmission is related to the effective wire tension, which is proportional to the amplitude of the tension. The sensing wires of the proposed sensor experience low effective tension.

To evaluate the reliability of the bending and force-sensing signals of the proposed multiparameter sensor, two separate experiments were conducted under different conditions: repetitive bending without contact force, and repetitive contact force loading at a constant bending angle. The reliability of the bending signals was tested through repetitive bending by the servo motor (Dynamixel MX-28, ROBOTIS). The range of repetitive bending was from 0° to 90°, with a period of 4 s and a speed of 10 RPM, for up to 10 000 cycles which took approximately 12 h as shown in Fig. 11(a). As depicted in Fig. 11(b), the Hall-effect sensor values for bending varied by 5.97°, with a standard deviation of 0.0572 up to 6000 cycles. After 6000 cycles, the sensor values decreased by 1° per 555 cycles owing to the mechanical degradation of the sensing wire and sheath.

The force-sensing output signal was evaluated by repeatedly compressing the membrane using a linear actuator with a constant displacement as illustrated in Fig. 11(c). The obtained results, shown in Fig. 11(d), indicate that the sensor was able to operate for a period of up to 10 000 cycles with no observable degradation or failure in performance. The sensor error for loading and unloading up to 6500 cycles was 0.2 N in the force scale, but the force-sensing output remained converged in the loading and unloading range after 6500 cycles. The results demonstrate the high reliability of the proposed sensor over an extended period, with no noticeable degradation or failure in the measured signals.

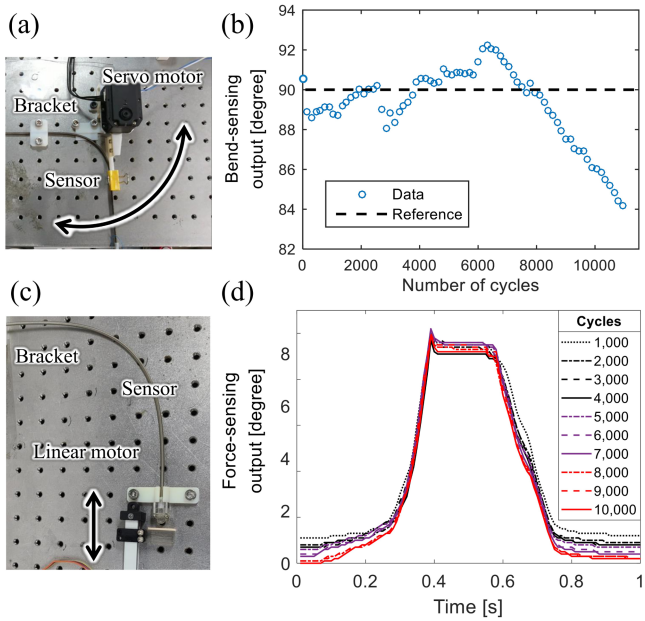

Fig. 11. Results of reliability tests. (a) Repetitive bending measurements performed without contact force. (b) Displacement measurement of bend-sensing wire up to 10 000 cycles at a 90° angle. (c) Repetitive loading of contact force at a constant bending angle. (d) Displacement measurement of force-sensing wire up to 10 000 cycles.

V. Applications

It is important to generate appropriate gripping forces based on the characteristics of various objects to enable tendon-driven robots to assist disabled individuals. For instance, when holding a rounded cup or a cylinder difficult to enclose with a hand, applying an adequate grasping force instead of overcompensating with a maximum grasping force can prevent the ejection of the object from the hand. Therefore, it is necessary to acquire fingertip force when the robotic hand or wearable hand robot grasps a target object.

We constructed two types of applications using sensor prototypes to demonstrate the potential of the proposed sensor in robotic systems. The first application is a robotic hand for proprioception, whereas the second is a tendon-driven soft wearable robot hand. In these applications, the sensor detects the contact and movement of the robots without requiring significant changes to the original robotic design.

A. Tendon-Driven Anthropomorphic Robotic Hand

Several robotic hands employ passive extensors with springs to reduce the number of actuators and realize a lightweight and noncomplex structure [32]. A recent paper proposed a kinesthetic feedback system of a prosthetic hand using a Bowden cable to detect the physical movement of closing of the hand [33].

1) Selection of an Elastomer Membrane: According to the study of force distribution in grasp taxonomy, a sensing range of 0–8 N was selected for the tip of the thumb, which is the force range of various types of grasps [34]. The membrane was characterized based on the thickness to determine the stiffness (k_{tip}) and estimate the sensor sensitivity and sensing range required by the robotic application. Three types of membrane specimens with different thicknesses (0.5, 0.8, and 1.3 mm) were fabricated and assembled to the end tip to clamp the side of a membrane.

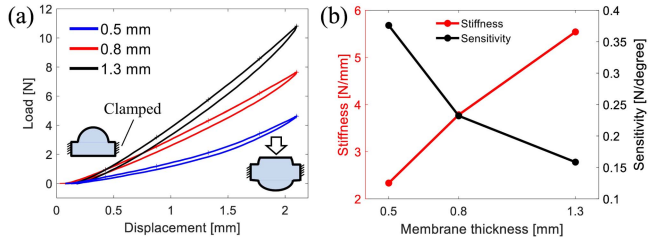

Fig. 12. Measurement results of elastomer membrane thickness repeated five times. (a) Applied load corresponding to membrane displacement, with the cross symbol representing the mean values. (b) Mean stiffness and sensitivity according to membrane thickness, showing tradeoff relationships.

Membrane specimens were tested through five cycles of compression tests until full deformation. Fig. 12(a) shows the relationship between the membrane displacement and load obtained through a compression test under a constant speed by using a tensile testing machine (Instron 5948). The sensitivity and sensing range were determined using the design parameters of the elastomer membrane of the end tip. Fig. 12(b) summarizes the relationship between the stiffness and the sensitivity in terms of membrane thickness. The mean stiffness increased in proportion to the thickness: 2.33 $N/$mm at 0.5 mm, 3.78 $N/$mm at 0.8 mm, and 5.54 $N/$mm at 1.3 mm, with a standard deviation of 0.005 $N/$mm, 0.03 $N/$mm, and 0.06 $N/$mm, respectively. The membrane sensitivity increased as the membrane thickness decreased: 0.375 $N/^\circ$ at 0.5 mm, 0.232 $N/^\circ$ at 0.8 mm, and 0.158 $N/^\circ$ at 1.3 mm. The sensitivity and the stiffness were estimated by linear regression, and the *R*-square values of each membrane were 0.971, 0.995, and 0.994 for thicknesses of 0.5, 0.8, and 1.3 mm, respectively. The maximum sensing range of the membranes is 4.63, 7.64, and 10.8 N at 0.5, 0.8, and 1.3 mm, respectively. Thus, a 1.3-mm-thick membrane was integrated into the anthropomorphic robotic hand to ensure a sensing range of 0–8 N.

2) Sensor Integration: The proposed sensor was embedded in an anthropomorphic robotic hand that required robust interconnection of the sensors [17]. The spring sheath was embedded in the finger as a passive extensor, which was designed in a previous study and allowed extension and sensing in a single structure, as shown in Fig. 13(a) and (b). The sensor passed through multiple joints of the finger and measured the accumulated bending angle of finger flexion.

We analyzed the pressure distribution to verify the application prospect of the embedded sensor by grasping a cylindrical object. The pressure values were measured using a pressure pad (pliance system, novel GmbH) that wraps around the 40 mm diameter cylinder, as shown in Fig. 13(c). When enclosing the cylinder, the integrated sensor detects the contact of the object and prevents the ejection of the grasped object because of the overflexion of the thumb by setting the contact force threshold of 3 N. The supplementary video shows that the robotic hand detects contact and measures the accumulated flexion/extension angle of the thumb. With the sensor electronics remotely separated from the end-effector, the anthropomorphic robotic hand can contact the watery environment as shown in Fig. 13(d).

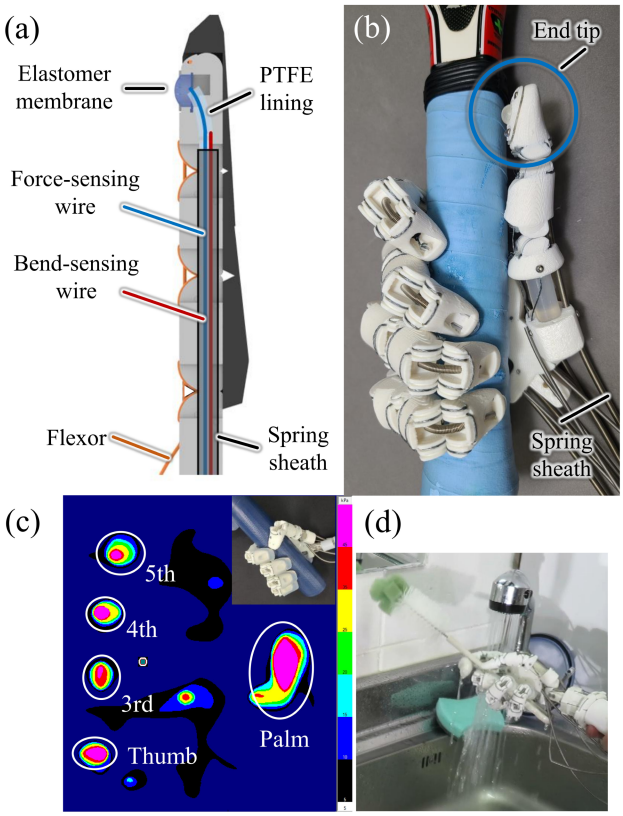

Fig. 13. Anthropomorphic robotic hand integrated with the proposed sensor: (a) schematic structure of the finger, (b) sensor-embedded robotic hand, (c) pressure distribution by grasping a cylindrical object, and (d) sensing in a water environment.

B. Tendon-Driven Soft Wearable Hand Robot

We implemented the proposed sensor in an Exo-glove Poly II, which is a polymer-based soft wearable robot for the hand with a tendon-driven actuation system [35]. A previous study measured the tendon tension from the load cell, tendon excursion length using motor encoders, and sheath bending angles to estimate the fingertip force with a machine learning model since the Exo-glove Poly II suffers from sensor integration issues, instead of directly attaching the tactile sensors on the fingertip [36]. Nevertheless, the indirect estimation of fingertip forces is by combining several measurements. However, it has limitations in simultaneous measurements.

The Exo-glove Poly II comprises a glove and spring sheaths with an underactuated tendon-driven mechanism. The glove consists of thimbles, finger bodies, straps, a dorsal body, a volar body, and a palm strap. The tendon paths for the index and middle finger extensions were located on the dorsal body of the glove. The proposed sensor was embedded in the existing extensor tendon path of the index finger, and the original spring sheath was utilized as a sensor structure; thus, the design of Exo-glove Poly II remained the same. Three types of wires pass through the extensor tendon path: a force-sensing wire, a bend-sensing wire, and an extensor tendon that operated the index finger extension, as shown in Fig. 14(a). The force-sensing wire was connected to the elastomer tip on the thimble of the glove and transmitted

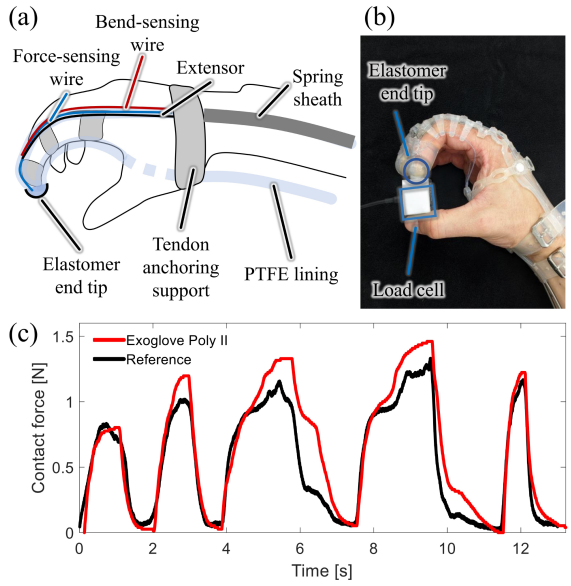

Fig. 14. Integration of the proposed sensor into a tendon-driven soft wearable glove (Exo-glove Poly II): (a) schematic of the glove structure. (b) Exo-glove Poly II with an elastomer end tip measuring fingertip force during a pinch grip, and (c) time-domain graph of reference force measurements (black line) and sensor output (red line) during five trials of pinch grip.

the deformation of the end tip. The bend-sensing wire was tied around the thimble to measure the flexion and extension angles of the index finger.

The elastomer tip ($10 \times 10 \times 4$ mm) for fingertip force sensing was embedded in the thimble of the finger body, as shown in Fig. 14(b). A more compliant material (Ecoflex 0030; Smooth-On, Inc.) compared to that of the glove body (KE-1300 T; Shin-Etsu Chemical Co., Ltd) was used for the elastomer tip. In this application, contact occurred after the finger flexion; therefore, simultaneous measurement of the contact force and bending angle information was rarely required. The relationship between the fingertip force and the sensor output was linearly determined as 0.150 $N/°$. The fingertip force of the Exo-glove Poly II with a pinch grip is plotted in Fig. 14(c) in the time domain with a sampling rate of 100 Hz, where the reference force was measured using a load cell. The fingertip force RMS error during the pinch grip is 0.18 N, indicating that Exo-glove Poly II can measure the contact force of the fingertip by only attaching a relatively light elastomer tip. Overall, the Exo-glove Poly II, integrated with the proposed sensor, accurately measures fingertip force during pinch grip with high sensitivity.

VI. Discussion

The proposed sensor has several characteristics that differentiate it from other sensors used for robotic applications, particularly in tendon-driven robots with inherent compliance.

1) *Low additional cost for sensor integration:* The proposed sensor utilized the Bowden cable of a tendon-driven robot, and the additional components for sensing are made of low-cost materials and can be manufactured using off-the-shelf components without using specialized fabrication techniques.
2) *Long mechanical transducer length:* The mechanical transducer length of the proposed sensor can be theoretically increased without limitation, but unmodeled properties may affect its characteristics if the length is significantly increased.
3) *Bending stiffness:* The bending stiffness of the sensor is determined by the stiffness of the helical coil and the tension of the sensing wires. Increasing the tension in the sensing wires and the diameter of the helical coil can contribute to the restoring force from the sensing wire, thereby increasing the bending stiffness. The bend stiffness profile can be adjusted by changing the radius of the spool and the spring constant.
4) *Environmental robustness:* The absence of electronic components on the sensor module ensures robustness to environmental conditions. The sensor components, such as the stainless steel, PTFE lining, and polymeric sensing wire, have high chemical and thermal resistance. Furthermore, the sensor is mechanically operated, which makes it suitable for use in environments with electromagnetic interference or when in contact with water.

VII. Conclusion

In this study, we presented the design and modeling of a contact force and bending sensor based on the characteristics of Bowden cables. The proposed sensor detected the displacement difference between the inner wires when the sheath bent and transmitted the information to a remotely separated sensor module. We improved the previous design of the Bowden cable angle sensor to enable measuring multiparameter of the bending angle and contact force. The developed sensor exhibited high linearity and repeatability of external force measurement at a constant bending angle. Importantly, the overall form factor remained the same, despite the addition of sensing components, because the elements were packaged in the compact sheath that fits within the tendon-driven robot structure.

The proposed sensor was integrated into several robotic devices by appending sensing wires to the sheath utilizing the original tendon path of the tendon-driven robot structure. We demonstrated that the sensor is affordable and straightforward to assemble and integrate.

For future research, sensor characterization with sheath and inner wires made of different materials could expand the potential applicability of the proposed sensor. Adopting various types of outer sheaths depending on the robotic application, such as PTFE sheaths in soft wearable gloves or polyvinyl chloride sheaths in bicycle brakes, could also be explored. Additionally, altering the materials of the force-sensing wire with low bending stiffness could reduce the nonlinear region that occurs under high contact force. These changes could support the integration of the sensor with not only end-effectors, such as robotic grippers or gloves, but also wire-driven surgical devices or lower limb wearable robots.

REFERENCES

[1] R. S. Dahiya, G. Metta, M. Valle, and G. Sandini, "Tactile sensing-from humans to humanoids," *IEEE Trans. Robot.*, vol. 26, no. 1, pp. 1–20, Feb. 2010.

[2] N. Yogeswaran et al., "New materials and advances in making electronic skin for interactive robots," *Adv. Robot.*, vol. 29, no. 21, pp. 1359–1373, 2015.

[3] A. M. Almassri et al., "Pressure sensor: State of the art, design, and application for robotic hand," *J. Sensors*, vol. 2015, 2015, Art. no. 12.

[4] M. Totaro, A. Mondini, A. Bellacicca, P. Milani, and L. Beccai, "Integrated simultaneous detection of tactile and bending cues for soft robotics," *Soft Robot.*, vol. 4, no. 4, pp. 400–410, 2017.

[5] T. Kim, S. Lee, T. Hong, G. Shin, T. Kim, and Y.-L. Park, "Heterogeneous sensing in a multifunctional soft sensor for human-robot interfaces," *Sci. Robot.*, vol. 5, no. 49, 2020, Art. no. eabc6878.

[6] Y. Yang and Y. Chen, "Innovative design of embedded pressure and position sensors for soft actuators," *IEEE Robot. Autom. Lett.*, vol. 3, no. 2, pp. 656–663, Apr. 2018.

[7] R. L. Truby et al., "Soft somatosensitive actuators via embedded 3D printing," *Adv. Mater.*, vol. 30, no. 15, 2018, Art. no. 1706383.

[8] R. P. Rocha, P. A. Lopes, A. T. De Almeida, M. Tavakoli, and C. Majidi, "Fabrication and characterization of bending and pressure sensors for a soft prosthetic hand," *J. Micromechan. Microeng.*, vol. 28, no. 3, 2018, Art. no. 034001.

[9] P. Weiner, C. Neef, Y. Shibata, Y. Nakamura, and T. Asfour, "An embedded,multi-modal sensor system for scalable robotic and prosthetic hand fingers," *Sensors*, vol. 20, no. 1, 2020, Art. no. 101.

[10] M. Grebenstein et al., "The hand of the DLR hand arm system: Designed for interaction," *Int. J. Robot. Res.*, vol. 31, no. 13, pp. 1531–1555, 2012.

[11] M. G. Catalano, G. Grioli, E. Farnioli, A. Serio, C. Piazza, and A. Bicchi, "Adaptive synergies for the design and control of the PISA/IIT softhand," *Int. J. Robot. Res.*, vol. 33, no. 5, pp. 768–782, 2014.

[12] H. In, B. B. Kang, M. Sin, and K.-J. Cho, "Exo-Glove: A wearable robot for the hand with a soft tendon routing system," *IEEE Robot. Autom. Mag.*, vol. 22, no. 1, pp. 97–105, Mar. 2015.

[13] B. B. Kang, H. Lee, H. In, U. Jeong, J. Chung, and K.-J. Cho, "Development of a polymer-based tendon-driven wearable robotic hand," in *Proc. IEEE Int. Conf. Robot. Automat.*, 2016, pp. 3750–3755.

[14] J. Choi, S. H. Ahn, C. Kim, J.-H. Park, H.-Y. Song, and K.-J. Cho, "Design of continuum robot with variable stiffness for gastrointestinal stenting using conformability factor," *IEEE Trans. Med. Robot. Bionics*, vol. 2, no. 4, pp. 529–532, Nov. 2020.

[15] C. Tawk, H. Zhou, E. Sariyildiz, M. In Het Panhuis, G. M. Spinks, and G. Alici, "Design, modeling, and control of a 3D printed monolithic soft robotic finger with embedded pneumatic sensing chambers," *IEEE/ASME Trans. Mechatron.*, vol. 26, no. 2, pp. 876–887, Apr. 2021.

[16] S. Oh et al., "Remote tactile sensing system integrated with magnetic synapse," *Sci. Rep.*, vol. 7, no. 1, pp. 1–8, 2017.

[17] S.-H. Kim, S. Oh, K. B. Kim, Y. Jung, H. Lim, and K.-J. Cho, "Design of a bioinspired robotic hand: Magnetic synapse sensor integration for a robust remote tactile sensing," *IEEE Robot. Autom. Lett.*, vol. 3, no. 4, pp. 3545–3552, Oct. 2018.

[18] L. K. Simone and D. G. Kamper, "Design considerations for a wearable monitor to measure finger posture," *J. Neuroeng. Rehabil.*, vol. 2, no. 1, pp. 1–10, 2005.

[19] P. Polygerinos, L. D. Seneviratne, R. Razavi, T. Schaeffter, and K. Althoefer, "Triaxial catheter-tip force sensor for MRI-guided cardiac procedures," *IEEE/ASME Trans. Mechatron.*, vol. 18, no. 1, pp. 386–396, Feb. 2013.

[20] T. Li, A. Pan, and H. Ren, "A high-resolution triaxial catheter tip force sensor with miniature flexure and suspended optical fibers," *IEEE Trans. Ind. Electron.*, vol. 67, no. 6, pp. 5101–5111, Jun. 2020.

[21] S. B. Kesner and R. D. Howe, "Design principles for rapid prototyping forces sensors using 3-D printing," *IEEE/ASME Trans. Mechatron.*, vol. 16, no. 5, pp. 866–870, Oct. 2011.

[22] S. B. Kesner and R. D. Howe, "Robotic catheter cardiac ablation combining ultrasound guidance and force control," *Int. J. Robot. Res.*, vol. 33, no. 4, pp. 631–644, 2014.

[23] U. Jeong and K.-J. Cho, "A novel low-cost, large curvature bend sensor based on a Bowden-cable," *Sensors*, vol. 16, no. 7, 2016, Art. no. 961.

[24] U. Jeong and K.-J. Cho, "Control of a Bowden-cable actuation system with embedded boASensor for soft wearable robots," *IEEE Trans. Ind. Electron.*, vol. 67, no. 9, pp. 7669–7680, Sep. 2019.

[25] F. Shahmiri and P. H. Dietz, "ShArc: A geometric technique for multi-bend/shape sensing," in *Proc. Conf. Hum. Factors Comput. Syst.*, 2020, pp. 1–12.

[26] M. Kaneko, T. Yamashita, and K. Tanie, "Basic considerations on transmission characteristics for tendon drive robots," in *Proc. IEEE 5th Int. Conf. Adv. Robot.' Robots Unstructured Environ.*, 1991, pp. 827–832.

[27] T. Kim, D.-m. Kim, B. J. Lee, and J. Lee, "Soft and deformable sensors based on liquid metals," *Sensors*, vol. 19, no. 19, 2019, Art. no. 4250.

[28] L. Teng, S. Ye, S. Handschuh-Wang, X. Zhou, T. Gan, and X. Zhou, "Liquid metal-based transient circuits for flexible and recyclable electronics," *Adv. Funct. Mater.*, vol. 29, no. 11, 2019, Art. no. 1808739.

[29] C. Votzke, U. Daalkhaijav, Y. Mengüç, and M. L. Johnston, "3D-printed liquid metal interconnects for stretchable electronics," *IEEE Sensors J.*, vol. 19, no. 10, pp. 3832–3840, May 2019.

[30] N. E. Dowling, S. L. Kampe, and M. V. Kral, *Mechanical Behavior of Materials*. New York, NY, USA: Pearson, 2013.

[31] U. Jeong, K. Kim, S.-H. Kim, H. Choi, B. D. Youn, and K.-J. Cho, "Reliability analysis of a tendon-driven actuation for soft robots," *Int. J. Robot. Res.*, vol. 40, no. 1, pp. 494–511, 2021.

[32] Y.-J. Kim, J. Yoon, and Y.-W. Sim, "Fluid lubricated dexterous finger mechanism for human-like impact absorbing capability," *IEEE Robot. Autom. Lett.*, vol. 4, no. 4, pp. 3971–3978, Oct. 2019.

[33] P. D. Marasco et al., "Neurorobotic fusion of prosthetic touch, kinesthesia, and movement in bionic upper limbs promotes intrinsic brain behaviors," *Sci. Robot.*, vol. 6, no. 58, 2021, Art. no. eabf3368.

[34] B. Abbasi, E. Noohi, S. Parastegari, and M. Žefran, "Grasp taxonomy based on force distribution," in *Proc. IEEE 25th Int. Symp. Robot Hum. Interact. Commun.*, 2016, pp. 1098–1103.

[35] B. B. Kang, H. Choi, H. Lee, and K.-J. Cho, "Exo-Glove poly II: A polymer-based soft wearable robot for the hand with a tendon-driven actuation system," *Soft Robot.*, vol. 6, no. 2, pp. 214–227, 2019.

[36] B. B. Kang et al., "Learning-based fingertip force estimation for soft wearable hand robot with tendon-sheath mechanism," *IEEE Robot. Autom. Lett.*, vol. 5, no. 2, pp. 946–953, Apr. 2020.

Sang-Hun Kim received the B.S. and Ph.D. degrees in mechanical and aerospace engineering from Seoul National University, Seoul, South Korea, in 2015 and 2022, respectively.

He has been a Postdoctoral Fellow with Soft Robotics Research Center, Seoul National University, in 2022. He is currently a Staff Engineer with Samsung Research, Samsung Electronics Co., Ltd. His current research interests include soft wearable robots, bionic hands, and cable-driven systems.

Useok Jeong received the B.S. and Ph.D. degrees in mechanical and aerospace engineering from Seoul National University, Seoul, South Korea, in 2010 and 2017, respectively.

He has been a Postdoctoral fellow with Soft Robotics Research Center, Seoul National University, in 2017. He is currently a Senior Researcher of Robotics R&D Group, Korea Institute of Industrial Technology. His research interests include cable-driven systems, soft robots, smart sensing, and actuation.

Kyu-Jin Cho (Member, IEEE) received the B.S. and M.S. degrees in mechanical engineering from Seoul National University, Seoul, South Korea, in 1998 and 2000, respectively, and the Ph.D. degree in mechanical engineering from the Massachusetts Institute of Technology, Cambridge, MA, USA, in 2007.

He was a Postdoctoral Fellow with Harvard Microrobotics Laboratory until 2008. He is a Professor of mechanical and aerospace engineering, the Director of BioRobotics Laboratory, Seoul National University, and the Director of Soft Robotic Research Center. His research interests include biologically inspired robotics, soft robotics, soft wearable devices, novel mechanisms using smart structures, and rehabilitation/assistive robotics.

Dr. Cho received the 2014 IEEE RAS Early Academic Career Award, 2014 ASME Compliant Mechanism Award, and 2013 KSPE Paik Am Award.